Detection of Deterioration of Furnace Walls Using Large-Scale Point-Clouds

Yuki Shinozaki[0000-0002-1991-633X][1], Keisuke Kohira[0000-0002-7692-0386][2]
and Hiroshi Masuda[0000-0001-9521-6418][3]

[1] The University of Electro-Communications, yuki.shinozaki@uec.ac.jp,
[2] The University of Electro-Communications, keisuke.kohira@uec.ac.jp
[3] The University of Electro-Communications, h.masuda@uec.ac.jp

Corresponding author: Hiroshi Masuda, h.masuda@uec.ac.jp

ABSTRACT

Blast furnaces are large industrial structures to produce iron. Since scaffolding and wearing of furnace walls are caused in their long lifecycle, furnaces have to be repeatedly inspected and renovated. In this paper, we discuss methods for detecting scaffolding and wearing on furnace walls using point-clouds. We detect scaffolding and wearing as differences between the original wall surface and measured points. However, it is not easy to estimate wall shapes with no scaffolding and wearing, because most blast furnaces were not precisely built as designed in drawings. Therefore, we introduce three different methods for estimating the original wall surfaces, and verify whether these methods can appropriately detect scaffolding and wearing regions from point-clouds.

Keywords: Point-Cloud, Deterioration Diagnosis, Terrestrial Laser Scanner.

1   INTRODUCTION

Blast furnaces are large industrial structures to produce iron. Since scaffolding and wearing of furnace walls are caused in their long lifecycle, furnaces have to be repeatedly inspected and renovated. In conventional diagnosis of furnaces, inspectors visually estimate the amount of scaffolding and wearing, and identify a need for maintenance of furnace walls. However, conventional diagnosis is strongly dependent on the skill of each inspector. Moreover, in the diagnosis by the inspector, the depth, width, and degree of deterioration are not quantitatively measured. In conventional diagnosis, it typically takes a week or more for determining regions to be repaired and roughly estimating the amount of repair material.

The state-of-the-art terrestrial laser scanners can capture dense point-clouds from large-scale facilities in a short time. They are promising to precisely estimate the amount of scaffolding and wearing of furnace walls. We define "*scaffolding*" as regions on which molten metal adhered and solidified. We also define "*wearing*" as regions from which the material of the wall was scraped off.

If the original shape of a furnace wall is known, the amount of deterioration can be obtained as the difference between the original wall shape and measured points. However, it is difficult to apply this method to actual furnace walls. One reason is that drawings of old blast furnaces are often lost. Even if the drawings exist, they often differ from the current shapes due to repeated renovation. To make

matters worse, actual blast furnaces were not constructed as precise rotational surfaces, even though they were originally designed as nominal rotational surfaces, such as cylinders and cones. This is because the precision required for construction is relatively low in the case of furnace walls. Therefore, the shapes of furnace walls cannot be represented as simple rotational surfaces in most cases. If we approximate the furnace wall with nominal surfaces, construction errors of the original wall will be incorrectly detected as scaffoldings or wearings.

To detect scaffolding and wearing on a furnace wall, it is very important to estimate wall shapes with no scaffolding and wearing. We call the original wall shape that has no scaffolding and wearing as the *reference surface*.

Many researchers have studied for extracting primitive surfaces from point-clouds. Nan, et al. [8] and Tang, et al. [11] extracting planes from point-clouds to reconstruct buildings. Masuda, et al. [5] and Kawashima, et al. [2] extracted cylinders and planes to reconstruct CAD models of pipe structures in engineering plants. Masuda, et al. [4] also extracted polygonal faces to reconstruct box shapes in engineering plants. However, these methods approximated object surfaces with nominal planes and cylinders, although actual shapes are not precise planes and cylinders.

Several researches have studied methods for extracting deterioration of large-scale facilities based on point clouds. Mizoguchi et al. [7] proposed a method for detecting wearing regions of bridge piers by supposing the original shapes as precise planes. They detected the aged deterioration as the difference between the ideal plane and the actual measured points. In this method, healthy regions with no wearings were manually selected, and the reference surfaces were calculated using points in healthy regions. Then, deterioration was calculated using the reference surfaces. However, their method is effective only when bridge piers are eroded very largely compared to construction errors. They showed that their method was effective for a bridge with severe salt damage. However, in cases of furnace walls, construction errors are often larger than scaffoldings and wearings.

Nespeca et al. [9] also proposed a method for detecting scaffolding and wearing by using local planes as reference surfaces, because a small region on a distorted planar surface could be approximated as nominal planes. However, this method is very sensitive to kernel sizes, which have to be determined considering the delicate balance of the degree of wall distortion, the sizes of scaffolding and wearing, and noise levels of measured points.

In this paper, we discuss methods for detecting scaffolding and wearing on furnace walls. We capture dense point-clouds from a large blast furnace, and detect scaffolding and wearing on the furnace wall using the point-clouds. Since several methods can be considered for estimating reference surfaces, we introduce three different methods for calculating reference surfaces, and then evaluate these methods by comparing results of detected scaffolding and wearing. First, we approximate reference surfaces as ideal cylinders and cones, which are calculated using the least-square method. Secondly, we calculate reference surfaces as a combination of overlapping local cylinders and cones. Thirdly, we calculate reference surfaces using constrained B-spline surfaces. We implement all the three methods and verify whether these methods can appropriately detect scaffolding and wearing on the furnace wall.

2   EXTRACTION OF FURNACE WALLS

2.1   Sections of Furnace Walls

In this research, point-clouds of a blast furnace were captured using a terrestrial laser scanner, FARO Focus 3D X130 [1], as shown in Fig. 1(a). We captured point-clouds inside the furnace container at 12 positions to reduce occluded regions, because there were a lot of structures in the furnace container. The point-clouds were registered using a commercial software. Fig. 1 (b) shows a single point cloud, and Fig. 1(c) shows registered point-clouds. The total number of points in the 12 point-clouds is about 446 million. The height of the furnace is about 23 m.

After laser scanning, each point-cloud was stored in the PTX format, which maintains 3D coordinates in the scanner-centered coordinate system. As shown in Fig. 1(a), the directions of laser beams are controlled by the azimuth angle θ and the zenith angle ϕ. Since points are sampled in equal angle intervals, points are ordered on a grid in (θ, ϕ) space. In the header of the PTX format, the numbers of

columns and rows of the 2D grid, and a registration matrix are described. Then, each scanner-centered coordinate (x, y, z) is stored in a 2D lattice manner.

Since each coordinate is on two-dimensional grid, a point-cloud can be easily converted into a wireframe model by connecting adjacent points. Fig. 2 shows a point-cloud and a converted wireframe model. Edges of the wireframe model are generated along grids of the two-dimensional lattice.

Then we calculate section points of wireframe models by slicing them using horizontal planes, as shown in Fig. 3(a). Furnace walls are typically made of rotational surfaces. Therefore, section curves become approximately circles. Since the number of points in all point-clouds is too large to process on a normal PC, each point-cloud is separately processed. As shown in Fig. 4, each point-cloud is converted
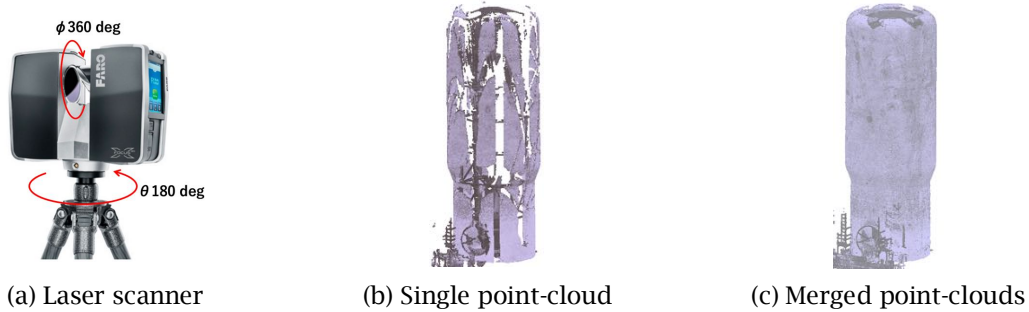

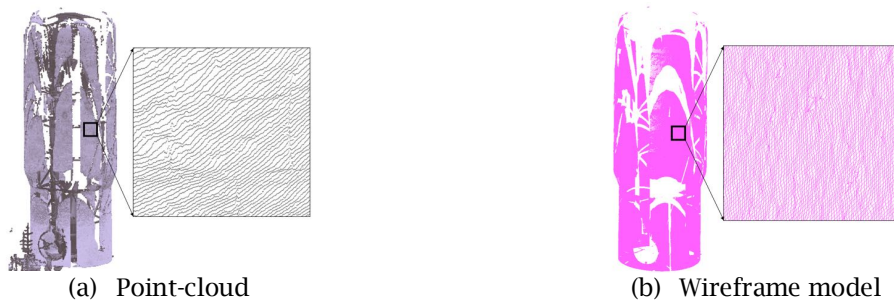(a) Laser scanner   (b) Single point-cloud   (c) Merged point-clouds
Fig 1: Measurement of furnace wall.

(a) Point-cloud   (b) Wireframe model
Fig 2: Conversion to wireframe model.

(a) Intersection with planes   (b) Merged intersection points   (c) Circle fitting
Fig. 3: Extraction of wall surfaces.

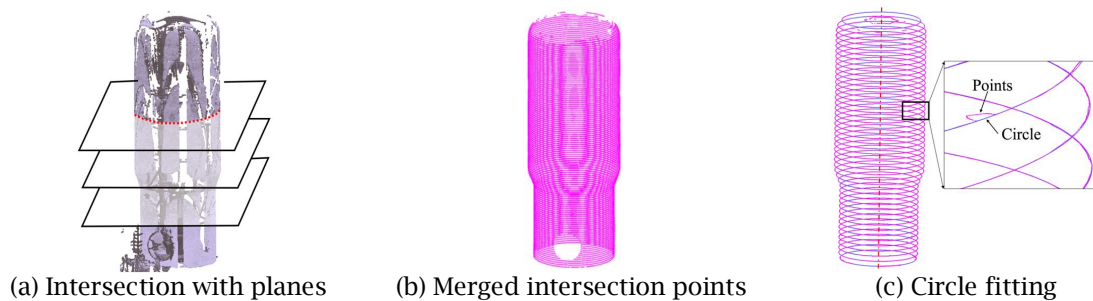Intersections at Position-1 + Intersections at Position-2 + Intersections at Position-3 + ·· + Intersections at Position-N → Merged intersections
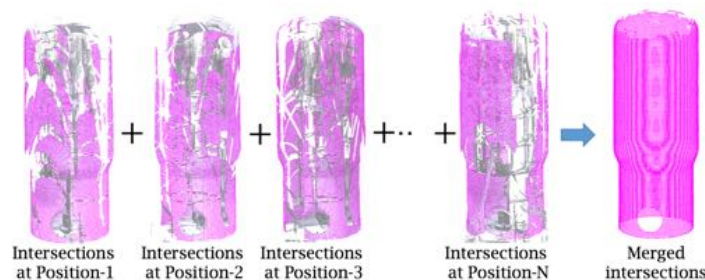
Fig. 4: Merging section points from multiple point-clouds.

to a wireframe model, and intersection points are calculated. Then section points from all point-clouds are merged.

When section points from multiple point-clouds are merged on each horizontal plane, a circle is detected from points using the RANSAC method. In the RANSAC method, three points are randomly selected and a circle equation is calculated using the three points. Then the number of points near the circle is counted. Since the furnace wall is not a precise rotational surface, the threshold for the RANSAC method should be large. In this research, the threshold was set at 10 cm. This process is iterated many times and the circle equation with the maximum number of points is recorded. When the maximum number exceeds a certain threshold, the detected circles are regarded as sections of the furnace wall.

When circles are calculated on horizontal planes, a straight line passing through the most center points is calculated. The straight line is regarded as the center line of rotational surfaces. Fig. 3(c) shows the center line by a one-dot chain line, which passes through the center points of section circles.

2.2   Initial Estimates of Rotational Surfaces

When section circles and the center line are calculated, cylinders, cones, and tori are segmented from the wall surface. We suppose the center line is the z axis, and the radii of circles can be represented as function R(z). As shown in Fig. 5(a), section circles are regarded as a cylinder surface when sequential circles have approximately same radii, and R(z) is a straight line parallel to the z axis. The radius of the cylinder is calculated as the average of circle radii. When the radii of circles are linearly increased or decreased, the circles can be regard as a cone. Then, R(z) is a straight line, and the taper of the cone can be calculated from the slope of the straight-line, as shown in Fig. 5(b). If R(z) can be approximated to a circle, the surface is regarded as a torus. Fig. 5(c) shows four surfaces generated from section circles. Tab.1 shows the size of each surface.

In this paper, we analyze deterioration of two cylinders S_1 and S_2, and a cone S_3. The segmented surfaces and their parameters are used as initial estimates of the reference surfaces.
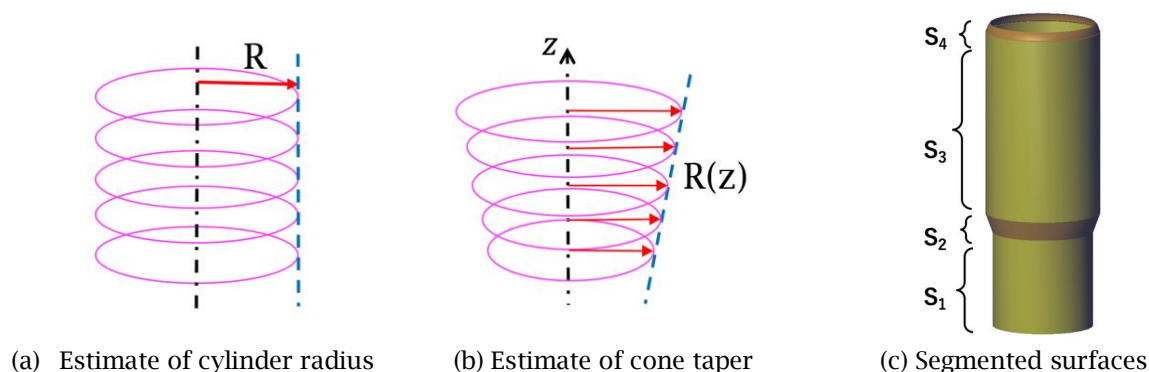

(a) Estimate of cylinder radius   (b) Estimate of cone taper   (c) Segmented surfaces
Fig. 5: Initial estimate of furnace walls.

Part	Surface Type	Height
S_1	Cylinder	7.20 m
S_2	Cone	1.10 m
S_3	Cylinder	13.75 m
S_4	Torus	0.85 m

Tab.1.   Height of segmented surfaces.

3 DETECTION OF DETERIORATION BASED ON ESTIMATED REFERENCE SURFACES

The amount of scaffolding and wearing can be calculated as differences between the reference surfaces and the original measured points. In our methods, reference surfaces are calculated using the section points. The system maintains only section points on RAM, because the number of points in original point-clouds are too large to store on RAM. In our example data, section points are calculated at the interval of 5 cm, and the total number of merged section points is 23.6 million.

To represent reference surfaces, we investigate three different types of surfaces; (1) nominal cylinders and cones, (2) overlapping strip-like surfaces, and (3) constrained B-spline surfaces. In the method (1), two nominal cylinders and a nominal cone are used as reference surfaces. In the method (2), distorted surfaces are locally approximated as cylinders or cones. In the method (3), they are approximated using free-form surfaces. In the following subsections, we describe the three methods.

3.1 Reference Surfaces Using Nominal Cylinders and Cones

Furnace walls are typically designed as rotational surfaces. In the case of the blast furnace shown in Fig. 1, the furnace wall was originally designed as two cylinders and a cone with a torus fillet. In the first method, we fit nominal cylinders and a cone to points on the furnace wall.

Several methods have been proposed to extract cylinders and cones from point-clouds. Lucacs, et al. [3] has proposed the faithful least-squares fitting to avoid singularity in nonlinear optimization. Masuda, et al. [6] extracted primitive surfaces from noisy points using the robust estimate. Schnabel, et al. [10] introduced the RANSAC method to robustly calculate primitive surfaces.

In this paper, we use the faithful least-squares fitting proposed by Lucacs, et al., because the initial estimates of surfaces are obtained from circle sections and therefore, outliers can be eliminated.

In this method, the objective function is defined as the squared sum of the modified distance function $d(\mathbf{s}, \mathbf{p}_i)$ as:

$$\underset{\mathbf{s}}{arg min} \sum_{i \in \Lambda} d(\mathbf{s}, \mathbf{p}_i)^2, \tag{1}$$

where $\mathbf{s}$ is parameters of a surface equation, and $\{\mathbf{p}_i\}$ ($i \in \Lambda$) is the measured points on the surface. This nonlinear optimization can be solved using the Levenberg-Marquardt method.

However, when the height of a cylinder or a cone is small, the axial direction tends to become unstable. Therefore, we constrain the direction of the axis to the direction of the center line obtained by the initial estimate. Fig. 6(a) shows two cylinders and a cone, which were calculated using the faithful least-squared fitting under the condition that the axial direction is fixed. We use these cylinders and a cone as the reference surfaces.

Then we calculate differences between the reference surfaces and measured points. We introduce a difference map to visualize deterioration. The nominal cylinders and cones can be converted into planes, when coordinates are represented using the cylindrical coordinate system (θ, ξ, r), as shown in Fig. 6 (c). The difference map is generated by discretizing θ and ξ, and store the difference of r on each pixel. The resolution of the difference map can be arbitrary determined. In our evaluation, the resolution was defined so that each pixel becomes less than 1 cm. The number of pixels of a difference map was about 400 million.

First, the depth map is generated by projecting the reference surfaces onto the θ-ξ plane. The values of r are described on pixels of the depth map. Then measured points are sequentially loaded from each file, and they are projected onto the θ-ξ plane. The value of r is compared to the one on the depth map, and the difference stored on the difference map if the difference is smaller than the threshold value. When multiple points are projected on the same pixel, the smallest difference is stored on the pixel.

Fig. 6 (c) shows a difference map visualized using RGB colors. The red and blue colors indicate wearing and scaffolding respectively, and the green color regions indicates no wearing and scaffolding.

Unfortunately, this difference map is not true, because large red and blue regions alternately appear, as shown in Fig. 7(a). This is because the actual furnace wall is not a precise rotational surface, and the distortion of the as-built wall was detected instead of wearing and scaffolding, as shown in Fig. 7(b).

This example shows that the as-built shape of the furnace wall is rather different from drawings, and the distortion from the nominal surfaces cannot be ignored to investigate wearing and scaffolding.
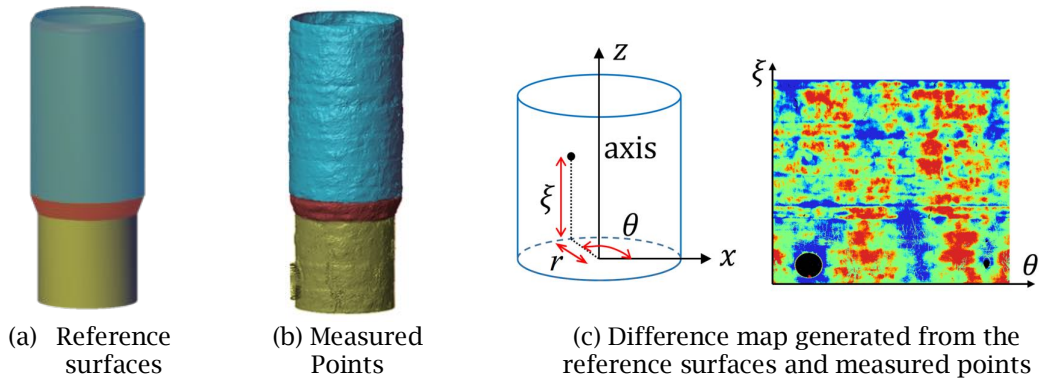

(a) Reference
surfaces

(b) Measured
Points

(c) Difference map generated from the
reference surfaces and measured points

Fig. 6: Calculation of scaffolding and wearing using nominal cylinders and a cone.

(a) Unnatural patterns on
the difference map.

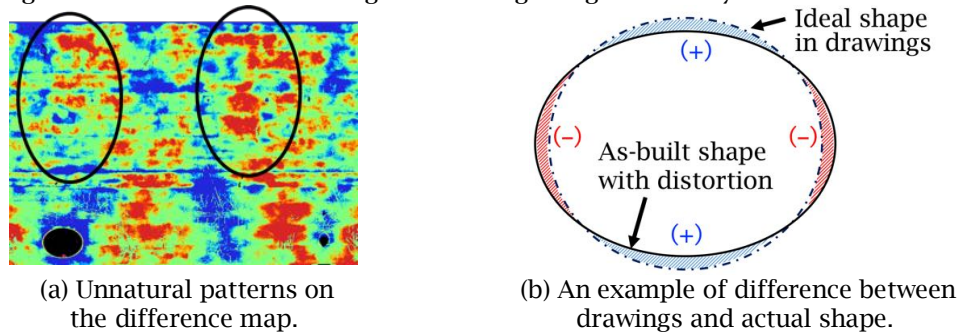(b) An example of difference between
drawings and actual shape.

Fig. 7: False deterioration on the difference map.

3.2 Reference Surfaces Using Overlapping Strip-like Surfaces

In the next step, we approximate the furnace wall using a set of strips of cylinders or cones to represent distorted walls, as shown in Fig. 8(a). In this method, points $\{\mathbf{p}_i\}$ on the wall are segmented in a strip manner, and points on each strip are separately fitted to a surface. We denote points on strip k as $\{\mathbf{p}_j\}$ $(j \in \Lambda_k)$. To avoid discontinuity at the borders of strips, we generate overlapping strips, as shown in Fig. 8(b).

However, surface fitting from small range points is very unstable when cylinders and cones are calculated using non-linear optimization. Thus, we calculate each surface using all points, but we add the large weight w only to the points on a strip, as shown in Fig. 8 (c). This method allows us to stably calculate segmented surfaces, each of which fits well to points on a strip.

Let $\mathbf{s}_k$ be the parameters of a surface for strip k. Then $\mathbf{s}_k$ can be calculated by solving the following equation:

$$\underset{\mathbf{s}_k}{\operatorname{argmin}}\left[w \sum_{i \in \Lambda_k} d(\mathbf{s}_k, \mathbf{p}_i)^2 + \sum_{i \notin \Lambda_k} d(\mathbf{s}_k, \mathbf{p}_i)^2\right] \quad (w \gg 1) \tag{2}$$

In this paper, we set the weight w to 100.

Once segmented surfaces are calculated for all strips, they are projected on the θ-ξ plane. When calculating a difference map, we linearly blend differences on overlapping regions to avoid discontinuity at the borders of strips. Suppose that strip a and strip b overlap on a difference map, as shown in Fig. 8(d). We denote l_a and l_b as the distances from the borders of strips a and b, and δ_a and δ_b as difference values on the pixel shown in black. Then the difference value δ is calculated as:

$$\delta = \frac{l_a \delta_b + l_b \delta_a}{l_a + l_b} \tag{3}$$

Fig. 9 shows difference maps generated from overlapping strips. Since the results depend on the number of strips, we calculated three difference maps using different numbers of strips. The three results show similar patterns of deterioration. These results do not contain unnatural strip-like patterns, which appeared in the difference map generated from nominal surfaces.

However, in all the three cases, unnatural large red regions are generated at the upper part of the furnace wall. This is because points are relatively sparse at far distances from the laser scanner, and therefore the reference surfaces are not well fitted to the upper part. In other words, the furnace wall is likely to be distorted in the vertical direction. Although it is possible to divide strips in the vertical direction, it is unstable to calculate partial surfaces using sparse points at the upper part. We will consider more flexible methods.
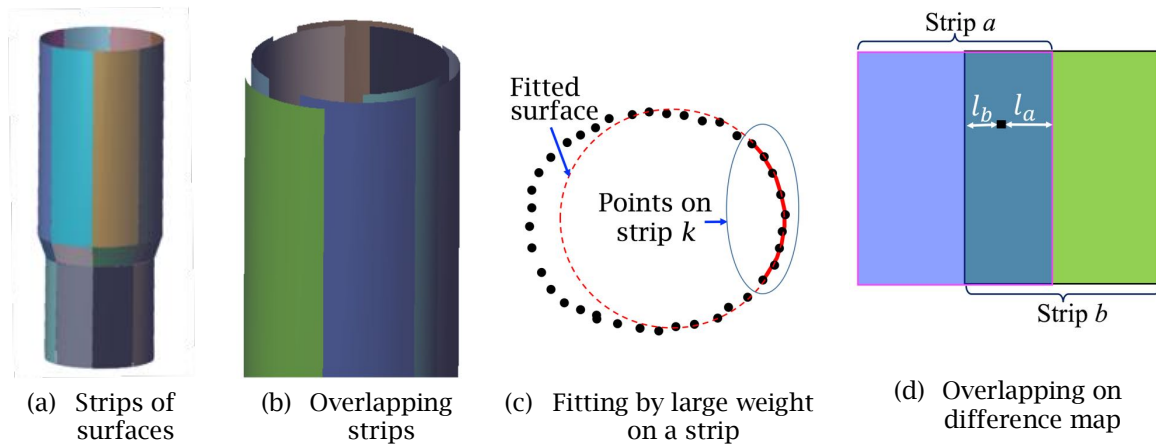

| (a) Strips of surfaces | (b) Overlapping strips | (c) Fitting by large weight on a strip | (d) Overlapping on difference map |

Fig. 8: Strips of cylinders and cones.

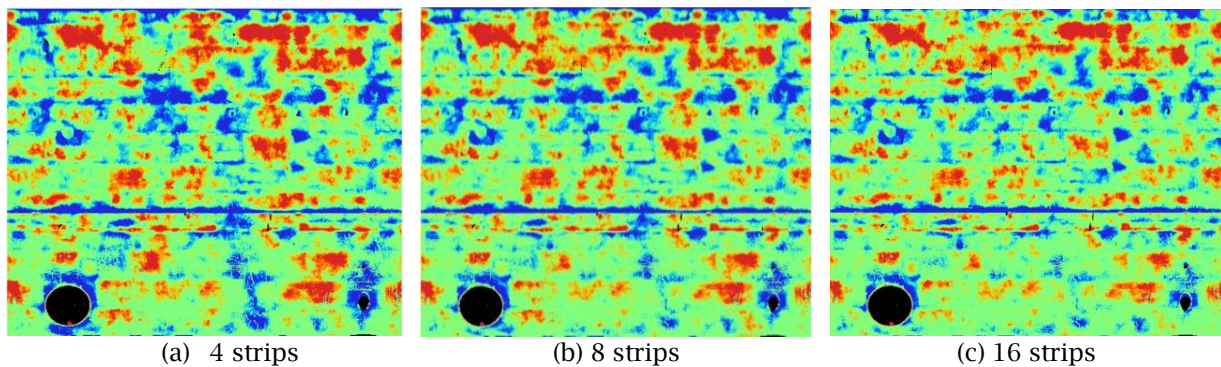| (a) 4 strips | (b) 8 strips | (c) 16 strips |

Fig. 9: Difference maps generated from overlapping strips.

3.3 Reference Surfaces Using Constrained B-Spline Surfaces

While the distortion of the furnace wall is relatively large-scale, the scaffolding and wearing tend to be local irregularities. Therefore, we consider low-resolution bi-cubic B-spline surfaces as reference surfaces.

To calculate a B-spline surface, we convert (x, y, z) coordinates into cylindrical coordinates (θ, ζ, r), as shown in Fig. 10(a). Then cylinders and cones are projected onto planar shapes, as shown in Fig. 10(b).

We segment the projected surface into a set of planar regions using the RANSAC method. Since planes are distorted (Fig.10 (c)), a large threshold value is used for the RANSAC method.

B-spline surface $\mathbf{S}(u,v)$ is fitted to each planar region. We suppose that $\{\mathbf{q}_{ij}\}$ are the control points, m_u and m_v are the numbers of control points in u and v directions, $\{\mathbf{p}_i\}$ $(i = 1,..,n)$ are measured points. In our method, parameters (u_i, v_i) of $\mathbf{p}_i$, are specified as (θ, ζ). The numbers of control points m_u and m_v have to be carefully determined to distinguish between the distortion and the deterioration. In this paper, we determine these numbers according to experiments.

In laser scanning, points are partially missing because of holes on the furnace wall and occluded regions. To avoid B-spline surfaces become indeterminate in missing regions, we add curvature terms to the objective function. In this paper, we simply represent curvature terms as linear equations. We calculate B-spline surfaces by minimizing the following objective function. The second term represents simplified curvature, which is introduced to avoid indeterminate solutions when points are partly missing [12]. The weight λ should be a small value. In this research, we specified $\lambda = 10^{-4}$.

$$\sum_{i=1}^{n}|\mathbf{S}(u_i,v_i) - \mathbf{p}_i|^2 + \frac{n\lambda}{m_u m_v}\left\{\sum_{i=1}^{m_u-2}\sum_{j=1}^{m_v}|\mathbf{q}_{i,j} - 2\mathbf{q}_{i+1,j} + \mathbf{q}_{i+2,j}|^2 + \sum_{i=1}^{m_u}\sum_{j=1}^{m_v-2}|\mathbf{q}_{i,j} - 2\mathbf{q}_{i,j+1} + \mathbf{q}_{i,j+2}|^2\right\} \qquad (4)$$

Difference maps are calculated using differences between B-spline surfaces and measured points. In our evaluation, we generate B-spline surfaces using different numbers of control points. Fig. 11 shows the results of difference maps.

Fig. 11 shows difference maps that were created using difference numbers of control points. In Fig. 11 (a), a small number of segments were used to represent B-spline surfaces. As with nominal cylinders and cones, unnatural patterns appeared. In Fig. 11 (b), the pattern is similar to the one of striped surfaces, because the degree of freedom is small in the vertical direction. As with stripped surfaces, unnatural patterns appear at the upper part of the furnace wall. In Fig. 11 (c), the numbers of control points are equal in u and v directions. In this case, appropriate patterns are obtained. In Fig. 11 (d), the resolution of B-spline surfaces is very high, and the reference surface is overfitting even to scaffolding and wearing. In this case, deterioration could not be distinguished from distortion.

These results show that the B-spline based method is suitable to detect deterioration if the number of control points are adequately determined.

In summary, B-spline surfaces can produce reasonable results when the adequate number of control points are used. Since the typical sizes of scaffolding and wearing regions are known, the adequate number of control points can be estimated using the number of control points per unit area. Stripped surfaces are also useful to detect deteriorations, but they may output false-positive results at distant regions.

Fig. 12 shows detailed points at which scaffolding and wearing regions were detected. The results show that out method could adequately detect scaffolding and wearing regions on the furnace wall.

In Tab.2, the calculation time is described for generating difference maps using the three methods. In our method, section points are calculated from all point-clouds, and then reference surfaces that fit the section points are calculated. The calculation time was measured on a PC with 16 GB RAM and a CPU of Intel Core i5-4440@3.10GHz×4. As shown in Tab. 2, reference surfaces could be calculated in practical time.

The total number of points	446 million points
The number of section points	23.6 million points

(a) The size of points

Nominal surfaces	103 sec
Striped surfaces (16 strips)	108 sec
B-spline surface (8 x 8 segments)	212 sec

(b) Calculation time
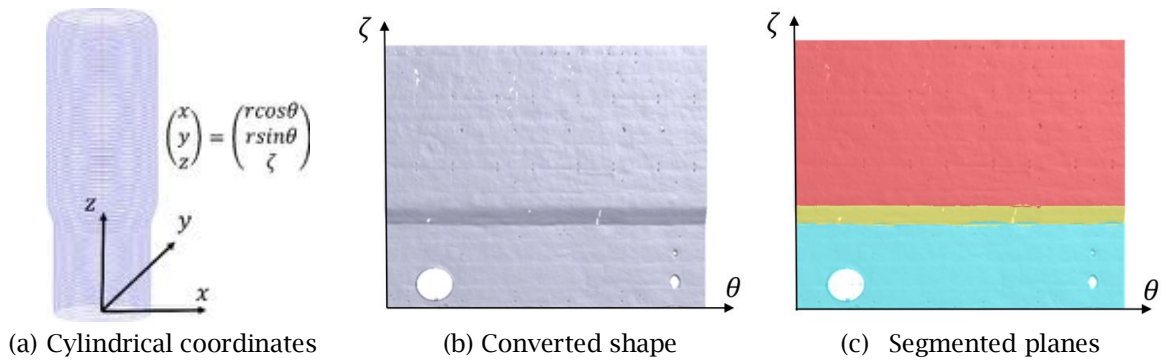
Tab. 2: Calculation time for generating difference maps

(a) Cylindrical coordinates   (b) Converted shape   (c) Segmented planes

Fig. 10: Difference map based on strips of surfaces.

(a) 3×1 segments   (b) 8×1 segments

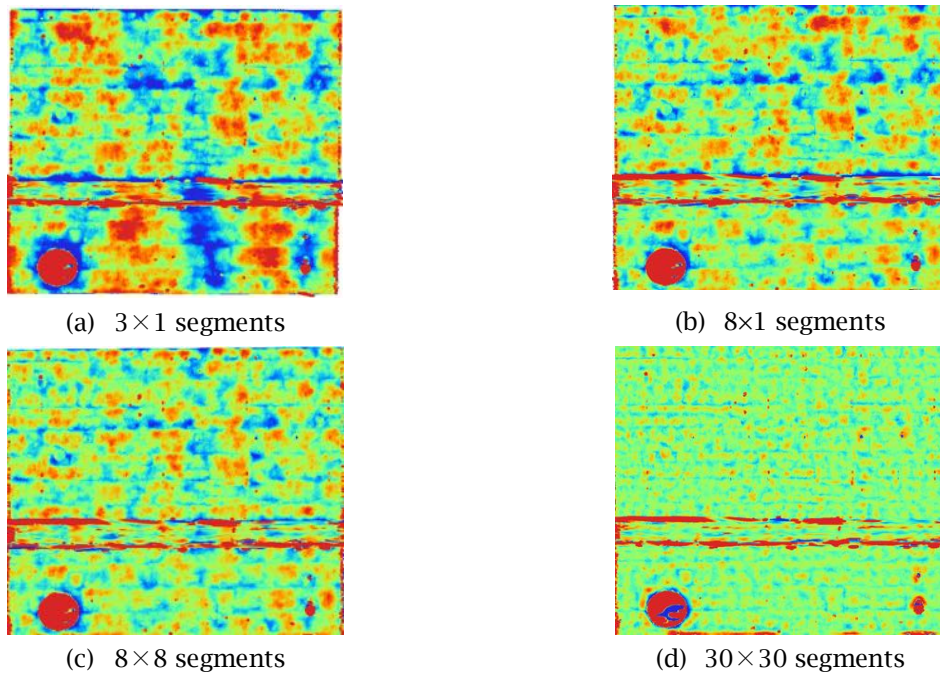

(c) 8×8 segments   (d) 30×30 segments

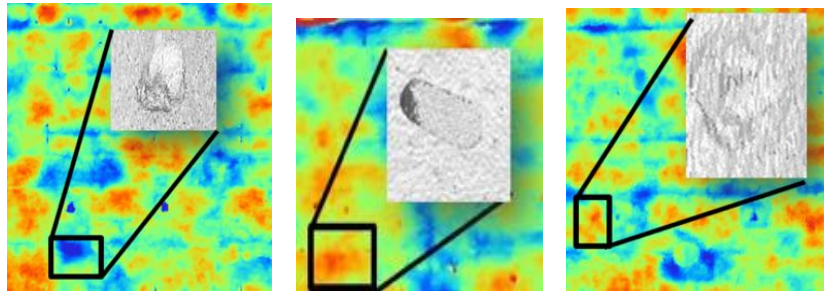Fig. 11: Difference map based on B-Spline surfaces with difference resolutions.

Fig. 12: Comparison of the difference map of B-spline surface with a surface model

4   ACCURACY EVALUATION OF PROPOSED METHODS

In this paper, we described three methods for calculating difference maps. In the previous section, we detected deteriorations from point-clouds of an actual blast furnace. However, unfortunately, we have no means to know the ground truth, because the blast furnace is currently in operation at all times, and it will be shut down only once every few year. Therefore, we evaluate the precision of our methods using simulated point-clouds.

In our experiments, we created multiple point-clouds by simulating laser scanning with different conditions. Then we investigated whether scaffolding and wearing regions could be detected by using the three methods described in this paper. When fitting overlapping strips to simulated points, we subdivided the furnace wall into sixteen strips. When fitting B-spline surfaces, we represented the furnace wall using B-spline surfaces with eight segments in each of the u and v directions.

Fig. 13 shows an example of simulated points, which are represented in the cylindrical coordinate system. In our implementation, the wall surface can be distorted using a sine wave. The wavelength and amplitude of the sine wave can be changed in the height and circumferential directions. Scaffolding and wearing regions are added on distorted surfaces in arbitrary width and depth. In Fig. 13(b), the depths of scaffolding and wearing regions become larger from left to right. Points are sampled from this surface, as shown in Fig. 13(c). Then normal distribution errors can be added to coordinates of points. In our experiments, the height and perimeter of the furnace wall is specified as 10 m, and the depths of scaffolding and wearing regions are 1 cm to 9 cm. The number of points is 500×500, and the standard deviation of noises is 3 mm.

First, we generated points on a non-distorted furnace wall, and calculated difference maps using the three methods. As shown in Fig. 14, all methods could correctly detect scaffolding and wearing regions.

Secondly, we distorted the furnace wall using the sine wave with a wavelength of 6.6m and an amplitude of 10 cm. The results are shown in Fig. 15. In this case, while the method based on the nominal surfaces failed to detect scaffolding and wearing regions, other two methods correctly detected them. These results show that overlapping strips and B-spline surfaces are effective for detecting deterioration when the furnace wall is distorted with a large wavelength.

Thirdly, we distorted the furnace wall using the sine wave with a wavelength of 6.6m and an amplitude of 50 cm. The results are shown in Fig. 16. In this case, while the methods based on the nominal surfaces and strip-like surfaces failed to detect scaffolding and wearing regions. The methods based on the B-Spline surfaces correctly detected them. These results show that only B-spline surfaces is effective for detecting deterioration when the furnace wall is distorted with a large wavelength which the amplitude is larger.

Tab. 3 summarizes the results of our evaluation. In this table, the results are shown as "*detected*" when all scaffolding and wearing regions could be detected. Otherwise, the results are shown as "*failed*". Only B-Spline surfaces could detect deteriorations in all cases. Overlapping strips could detect deteriorations only when the amplitude of distortions is small.

Whether a certain region needs to be repaired depends on both depth and area of deterioration. As far as we interviewed, there was no clear criteria for the depth and area, but inspectors thought that the depth at which repair is necessary is about 5 cm or more. Therefore, overlapping strips and B-spline surfaces could be used to detect practical sizes of scaffolding and wearing regions.

	No distortion	Distortion with small depth	Distortion with large depth
Nominal surfaces	Detected	Failed	Failed
Overlapping strips	Detected	Detected	Failed
B-Spline surfaces	Detected	Detected	Detected

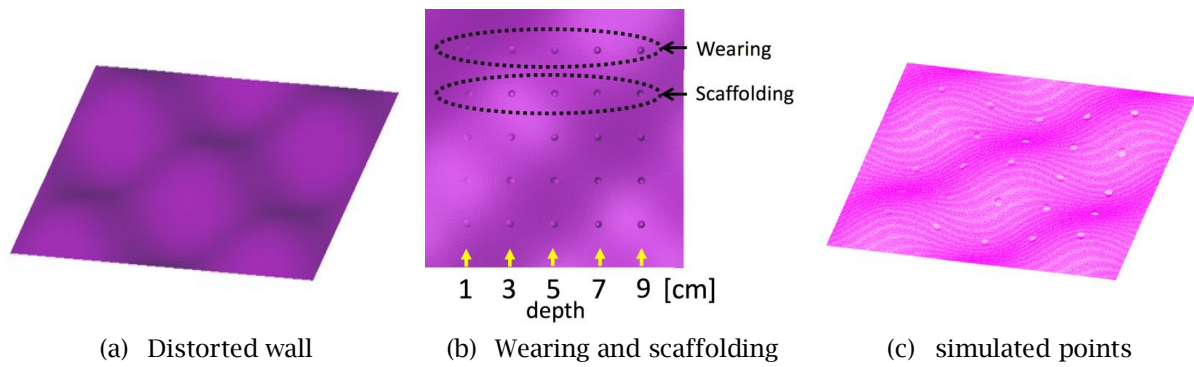Tab. 3: Results of detection of deterioration in simulated point-clouds

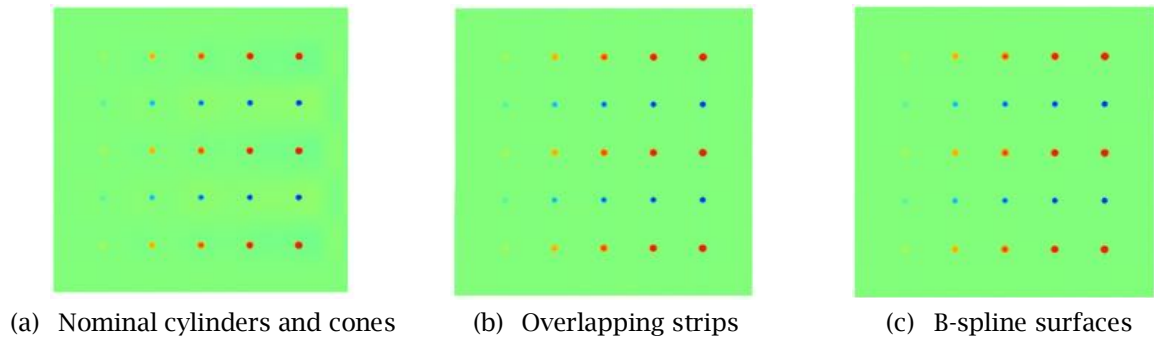(a) Distorted wall   (b) Wearing and scaffolding   (c) simulated points

Fig. 13: Simulated point-cloud

(a) Nominal cylinders and cones   (b) Overlapping strips   (c) B-spline surfaces

Fig. 14: Difference maps of the non-distorted furnace wall.

(a) Nominal cylinders and cones   (b) Overlapping strips   (c) B-spline surfaces
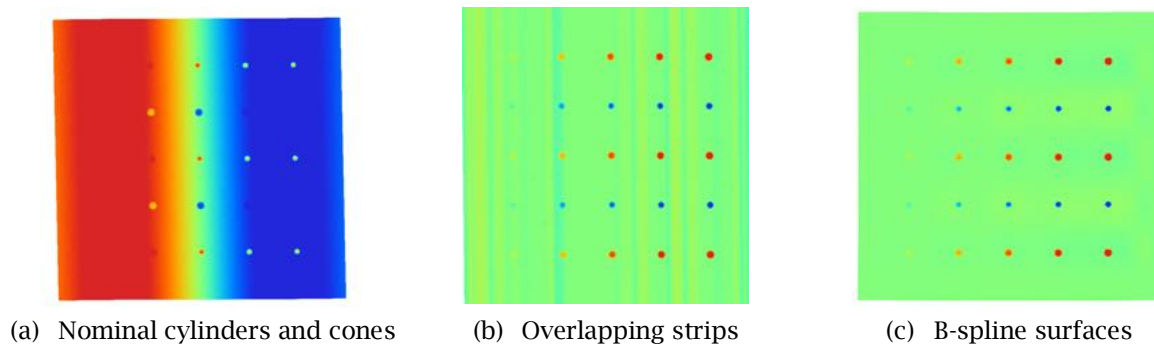
Fig. 15: Difference maps of the furnace wall distorted with small amplitude.

(a) Nominal cylinders and cones   (b) Overlapping strips   (c) B-Spline surfaces
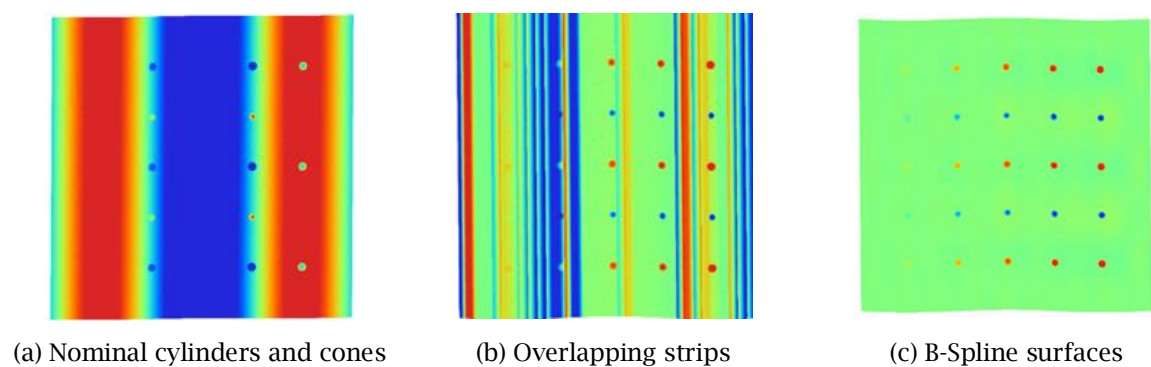
Fig. 16: Difference maps of the furnace wall distorted with large amplitude.

5   CONCLUSION

In this paper, we proposed methods for diagnosing scaffolding and wearing of furnace walls. We detected scaffolding and wearing as differences between the reference surfaces and measured points. To calculate reference surfaces, we introduced three types of surfaces; (1) nominal cylinders and cones, (2) overlapping strip-like surfaces, and (3) constrained B-spline surfaces. We implemented the three methods and evaluated whether these methods could appropriately detect scaffolding and wearing on furnace walls. When we used nominal cylinders and cones as the reference surfaces, distortion of furnace walls was extracted instead of scaffolding and wearing, and deterioration could not be properly identified. When we fitted strip-like surfaces to points, scaffolding and wearing could be extracted, but unnatural artifacts appeared at the upper part of the furnace wall. Finally, we calculated scaffolding and wearing regions using constrained B-spline surfaces. This method could extract scaffolding and wearing of furnace walls when the number of control points was properly specified.

In future work, we would like to investigate the ground truth of actual scaffolding and wearing. In addition, we would like to enhance methods so that small deterioration such as rust on structure can be robustly extracted.

REFERENCES

[1] FARO Laser Scanner Focus 3D X130, http://www.faro.com, 2014.r

[2] Kawashima, K.; Kanai, S.; Date, H.: As-Built Modeling of Piping System from Terrestrial Laser Scanned Point Clouds Using Normal-Based Region-Growing, Journal of Computational Design and Engineering, 1(1), 2014, 13-26. http://dx.doi.org/10.7315/JCDE.2014.002

[3] Lukacs, G.; Marshall, A.D.; Martin, R.R.: Faithful Least-Squares Fitting of Spheres, Cylinders, Cones and Tori for Reliable Segmentation, 5th European Conference on Computer Vision, 1998, 671–686.

[4] Masuda, H.; Niwa, T.; Tanaka, I.; Matsuoka, R.: Reconstruction of Polygonal Faces from Large-Scale Point-Clouds of Engineering Plants, Computer-Aided Design and Applications, 12(5), 2015, 555-563. http://dx.doi.org/10.1080/16864360.2015.1014733

[5] Masuda, H.; Tanaka, I.: As-Built 3D Modeling of Large Facilities Based on Interactive Feature Editing, Computer-Aided Design & Applications, 7(3), 2010, 349-360. http://dx.doi.org/10.3722/cadaps.

[6] Masuda, H.; Tanaka, I.: Extraction of Surface Primitives from Noisy Large-Scale Point-Clouds, Computer-Aided Design and Applications, 6(3), 2009, 387-398. http://dx.doi.org/10.3722/cadaps. 2009.387-398

[7] Mizoguchi, T.; Koda, Y.; Iwaki, I.; Wakabayashi, H.; Kobayashi, Y.; Shirai, K.; Lee, H. S.: Quantitative Scaling Evaluation of Concrete Structures Based on Terrestrial Laser Scanning, Automation in Construction, 35, 2013, 263-274. http://dx.doi.org/10.1016/j.autcon.2013.05.022

[8] Nan, L.; Sharf, A.; Zhang, H.; Cohen-Or, D.; Chen, B.: SmartBoxes for Interactive Urban Reconstruction. ACM Transactions on Graphics, 29(4), 2010, 93. http://dx.doi.org/10.1145/1778765.1778830

[9] Nespeca, R.; De Luca, L.: Analysis, Thematic Maps and Data Mining from Point Cloud to Ontology for Software Development, ISPRS-International Archives of the Photogrammetry, Remote Sensing and Spatial Information Sciences 2016, 347-354. http://dx.doi.org/10.5194/isprs-archives-XLI-B5-347-2016

[10] Schnabel, R.; Wahl, R.; Klein, R.: Efficient RANSAC for Point-Cloud Shape Detection, Computer Graphics Forum, 26(2), 2007, 214-226. http://dx.doi.org/10.1111/j.1467-8659.2007.01016.x

[11] Tang, P.; Huber, D.; Akinci, B.; Lipman, R.; Lytle, A: Automatic Reconstruction of As-Built Building Information Models from Laser-Scanned Point Clouds: A Review of Related Techniques, Automation in Construction, 19(7), 2010, 829-843. http://dx.doi.org/10.1016/j.autcon.2010.06.007

[12] Weiss, V.; Andor, L.; Renner, G.; Varady, T.; Advanced Surface Fitting Techniques," Computer Aided Geometric Design, 19(1), 2002, 19-42. https://doi.org/10.1016/S0167-8396(01)00086-3